



# CHORUS

This is the accepted manuscript made available via CHORUS. The article has been published as:

## Melting Can Hinder Impact-Induced Adhesion

Mostafa Hassani-Gangaraj, David Veysset, Keith A. Nelson, and Christopher A. Schuh

Phys. Rev. Lett. **119**, 175701 — Published 25 October 2017

DOI: [10.1103/PhysRevLett.119.175701](https://doi.org/10.1103/PhysRevLett.119.175701)

# Melting Can Hinder Impact-Induced Adhesion

Mostafa Hassani-Gangaraj<sup>1</sup>, David Veysset<sup>2,3</sup>, Keith A. Nelson<sup>2,3</sup>, Christopher A. Schuh<sup>1\*</sup>

<sup>1</sup>Department of Materials Science and Engineering, MIT, Cambridge, Massachusetts 02139, USA.

<sup>2</sup>Institute for Solider Nanotechnologies, MIT, Cambridge, Massachusetts 02139, USA.

<sup>3</sup>Department of Chemistry, MIT, Cambridge, Massachusetts 02139, USA.

\*Correspondence to: schuh@mit.edu

## Abstract

Melting has long been used to join metallic materials, from welding to selective laser melting in additive manufacturing. In the same school of thought, localized melting has been generally perceived as an advantage, if not the main mechanism, for adhesion of metallic microparticles to substrates during supersonic impact. Here, we conduct the first *in-situ* supersonic impact observations of individual metallic microparticles aimed at the explicit study of melting effects. Counter-intuitively, we find that under at least some conditions melting is disadvantageous and hinders impact-induced adhesion. In the parameter space explored, i.e.  $\sim 10\ \mu\text{m}$  particle size and  $\sim 1\ \text{km/s}$  particle speed, we argue that the solidification time is much longer than the residence time of the particle on the substrate, so that re-solidification cannot be a significant factor in adhesion.

## Text

Understanding materials physics under impact has motivated extensive research in areas ranging from asteroid strikes [1] and ballistic deposition [2] to mechanochemical synthesis [3], materials failures [4,5], structural modification [6] and phase transformation [7]. Less conventionally, three decades ago, metallic powder particles were first observed to bond to metallic substrates under supersonic-impact conditions at low temperatures [8]. The notion of impact-induced adhesion, thereafter, has been implemented in powder processing through kinetic deposition or cold spray [9,10]. Kinetic deposition has proven successful in making coatings [11–13], in reclaiming damaged metallic surfaces [14], and in additively manufacturing bulk metallic materials [15].

In this area of impact science, researchers have repeatedly observed a material-dependent critical velocity [16,17], a threshold above which supersonic particles change their mode of interaction with the substrate from rebound to adhesion. A variety of proposals including adiabatic shear instability [16], oxide layer break-up [18], diffusion [19] and localized melting [20] have been put forth to explain the underlying mechanism(s) of impact-induced adhesion, each of which enjoys partial support from observational data. For instance, sharp jumps observed in temperature and strain in Lagrangian impact simulations have been used to support an argument for adiabatic shear localization [16,21]. Experimental measurements of reduced oxide content in cold spray coatings as compared to initial powder feedstock underpins an argument for oxide layer break-up [22]. Small spherical ejecta found in the coating [20] or intermetallic detected at the interface [23] suggest localized melting or interdiffusion.

More consensus, however, has been attained around post-mortem observations of material jets around the periphery of adhered particles [16,24,25]. We have recently, for the first time, conducted *in-situ* observations of the impact behavior of individual supersonic metallic microparticles below and above the critical velocity and found that material ejection and jetting are crucial for adhesion [26]. We argued that neither shear localization nor melting are needed to account for material ejection. Rather, it can arise from

44 the interaction of the impact-induced pressure wave with the contact periphery of the particle. As a result,  
45 we found that the critical adhesion velocity is directly related to the bulk speed of sound [26]. In our  
46 view, the key feature is a fast-traveling pressure wave that drives material ejection and jetting when it  
47 interacts with the leading edge of an impacting particle just a few nanoseconds after the first contact.  
48 Subsequently, oxide layer break-up, shear localization, melting and resultant viscous flow might be, in  
49 fact, trailing consequences of extensive jetting.

50 Our focus on impact-induced-adhesion being a pressure-driven phenomenon therefore generally suggests  
51 that temperature rise—and by extension melting—need not adopt a critical importance in this context.  
52 The purpose of the present work is to take an additional significant step forward in this line of reasoning,  
53 by targeting the process of impact melting specifically to evaluate its role in adhesion. Our approach in  
54 conducting impact adhesion experiments differs from the more common use of spray nozzles, which  
55 includes many complex variables that we wish to eliminate from consideration. For example, in a typical  
56 experiment where expansion of a hot carrier gas accelerates thousands of particles together, the complex  
57 heat transfer and particle interactions lead to a general lack of specific knowledge on individual particles'  
58 velocity, size and temperature at the point of impact.

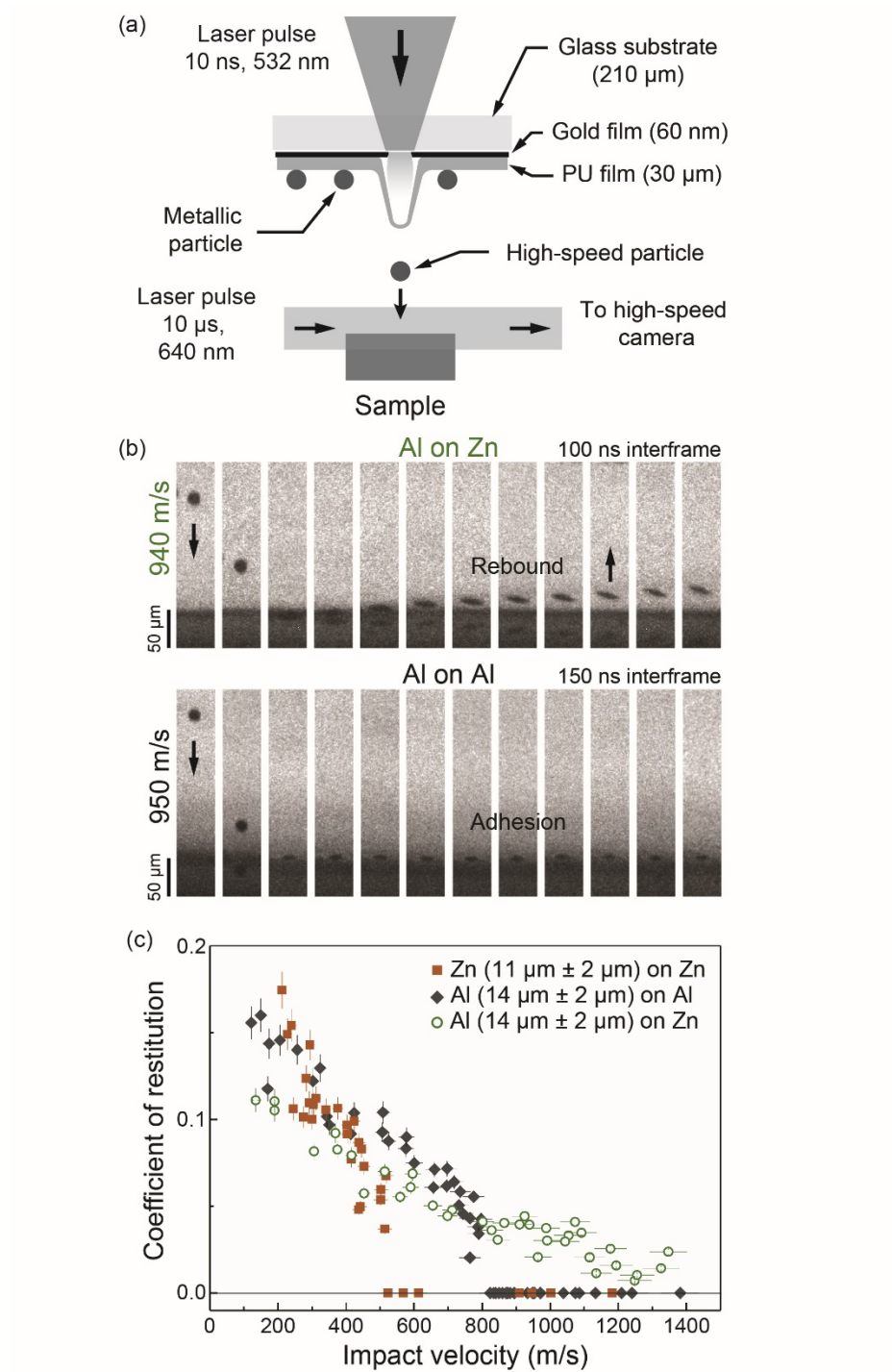
59 Here, on the other hand, we use an in-house-designed microscale ballistic test platform to accelerate  
60 individual micrometer-size metallic particles with well-defined size and well-controlled temperature, to  
61 have them impact a substrate, and to record the entire deformation, rebound or adhesion process in real  
62 time. What is more, our approach allows us to make a one-to-one correspondence between our post-  
63 mortem observations of the adhered particles/impact residue and the instant of impact. As shown  
64 schematically in Fig. 1(a), a laser excitation pulse is focused onto a launching pad assembly on top of  
65 which metallic particles are sitting. Through ablation of a gold layer and rapid expansion of an  
66 elastomeric polyurea film, single particles are launched toward a metallic substrate. We use a high-frame-  
67 rate camera and a synchronized quasi-cw laser imaging pulse to observe the particle approach and impact  
68 on the substrate in real time. More details regarding the launching pad assembly preparation, the optical  
69 setup, and the image analysis have been reported [27].

70 Figure 1(b) shows some exemplar *in-situ* images that we captured for individual supersonic microparticle  
71 impacts. The top image series shows a 15- $\mu\text{m}$  Al particle as it approaches a Zn substrate, impacts it at 950  
72 m/s, and undergoes extensive plastic deformation evidenced by the flattening of the rebounding particle.  
73 The bottom image series, on the other hand, shows a 15- $\mu\text{m}$  Al particle impacting an Al substrate with  
74 virtually the same velocity but adhering to the substrate. We have conducted many such experiments with  
75 a wide range of impact velocities for Al impact on Al, Zn impact on Zn, and Al impact on Zn. We  
76 measured the rebound and impact velocities for each impact and calculated the ratio between the two,  
77 known as the coefficient of restitution (CoR). Figure 1(c) shows the CoR as a function of impact velocity.  
78 The apparent linear decrease in the coefficient of restitution is followed by a sharp decline to zero,  
79 indicating particle adhesion, for Al and Zn particles impacting matched materials. This reveals the  
80 existence of the critical velocity for adhesion for these cases.

81 In contrast, for Al impacting on Zn, we have never observed a single Al particle adhering to Zn even at  
82 very high impact velocities, close to 1400 m/s. While the Al-on-Al and Zn-on-Zn data points deviate from  
83 linearity in a concave-downward fashion and fall to zero with many clear observations of adhesion, the  
84 Al-on-Zn data points deviate from linearity in a concave-upward fashion instead. They apparently plateau  
85 at a roughly constant non-zero CoR value at the high velocity range. Although these velocities are far  
86 beyond the critical adhesion velocity for both of the two constituent metals, there is apparently no critical  
87 adhesion velocity, at least over the studied range, for the mismatched Al/Zn pair. For a second, similar

88 mismatched pair (Al impacting Sn, see Fig. SM1 in Supplemental Material [28]) we see the same effect  
 89 but to even higher velocities.

90



91

92 FIG. 1. *In situ* observation of microparticle supersonic impact. (a) Experimental platform for  
 93 microparticle impact test and real-time imaging. (b) Multi-frame sequences with 5 ns exposure times

94 showing 15- $\mu\text{m}$  Al particle impacts on Zn substrate (top) and Al substrate (bottom) at 940 m/s and 950  
95 m/s (resp.) impact velocity. The micro-projectile arrives from the top of the field of view. It rebounds  
96 after impacting on Zn, but adheres to Al. (c) Coefficient of restitution for Al microparticle impacts on Al  
97 and Zn as well as Zn microparticle impacts on Zn. The coefficient of restitution is equal to zero above the  
98 critical velocity.

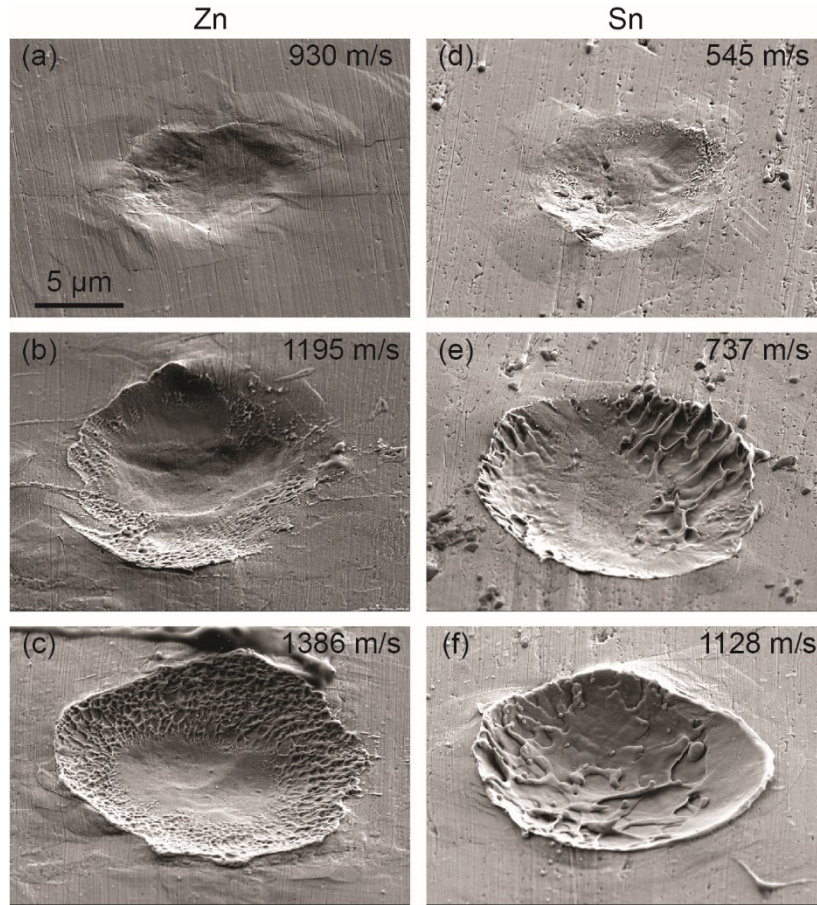
99

100 This is an anomalous finding and somewhat unexpected in light of the normal behavior of the Al-Al and  
101 Zn-Zn data. Site-specific observations of such impacts enable us to make a one-to-one correspondence  
102 between impact residue and the recorded impact event in the  $\sim 10$  ns-10  $\mu\text{m}$ -1 km/s time-size-velocity  
103 parameter space. The scanning electron microscope (SEM) images, shown in the left column of Fig. 2,  
104 correspond to three impressions left behind after impacts of Al particles on Zn substrates at 930, 1195,  
105 and 1368 m/s. An impact at 930 m/s left an appreciable indentation behind. The surface morphology  
106 inside the indentation is similar to that of the undeformed substrate outside; the substrate has been  
107 deformed plastically but not melted and resolidified. With further increase in impact velocity, a ring with  
108 a netlike structure—a signature of melting and rupture through a Rayleigh-Taylor instability [29]—  
109 emerged close to the indentation edge. Energy dispersive spectroscopy (EDS) analysis (see Fig. SM2 in  
110 [Supplemental Material \[28\]](#)) of the impacted area confirmed that the netlike structure consists of Zn  
111 substrate only, with no measurable contribution from the Al particle. In other words, it is the Zn substrate  
112 that undergoes melting and re-solidification, and not the Al particle, in line with the fact that Zn has a  
113 lower melting temperature than Al (693 vs. 933 K). The ring is only partial at the lower impact velocity  
114 but complete at the higher velocity. Interestingly, the impact velocity range causing melting is the same  
115 for which we observed the plateau of low but nonzero CoR values in Fig. 1(c).

116 Based on these observations, we propose that the anomalous lack of adhesion in this case is caused by the  
117 emergence of melting, which hinders impact-induced adhesion. To further confirm this, we conducted the  
118 same experiments with the same Al microparticles but with a Sn substrate. Because of its lower specific  
119 heat and melting temperature, we expected Sn to be more susceptible to melting than Zn in our  
120 microparticle impact events. SEM images in the right column of Fig. 2 show three indentations on a Sn  
121 surface with increasing impact velocities. The same trend holds for this situation, albeit at much lower  
122 impact velocities for Sn than for Zn (by about 500 m/s) as expected. At 1128 m/s the entire impact region  
123 underwent melting and re-solidification; it is interesting that even a high-velocity impact producing such a  
124 large extent of melting could not lead to the adhesion of the impacting particle on the substrate.

125 While we cannot rule out a possible second change in behavior that admits adhesion at velocities above  
126 the range we are able to study here, the trends in the data suggest that more extensive melting does  
127 nothing to improve adhesion. This is in spite of the fact that melting should promote chemical  
128 interactions between particle and substrate; whereas there is little solid solubility between these  
129 mismatched pairs, in the liquid Al-Zn is fully miscible and Al-Sn attains full miscibility if there is  
130 sufficient superheat in the liquid [30]. Similarly, the surface energy of Al is  $1.16 \text{ J/m}^2$ , and that of both Zn  
131 ( $0.99 \text{ J/m}^2$ ) and Sn ( $0.7 \text{ J/m}^2$ ) are much lower [31], which should correlate with a significant tendency to  
132 chemical mixing. Thus, as we increase the velocity to 1.4 times the threshold for melting in Al-Zn, we  
133 expect more chemical interaction that would favor bonding, but see no hint of adhesion. In the case of  
134 Al-Sn it is even more stark: even at velocities up to 2.25 times the melting onset, we find no cases of  
135 adhesion.

136



137

138 FIG. 2. SEM observation of Al microparticle supersonic impact induced-indentations on Zn substrate at  
 139 930 (a) 1195 (b) and 1386 (c) m/s velocities along the impact induced-indentations on Sn at 545 m/s (d),  
 140 737 (e) and 1128 (f) m/s velocities. Even though the substrate melted at increasing impact velocities,  
 141 melting clearly did not lead to adhesion.

142

143 These observations, far from supporting impact-induced melting as an adhesion mechanism, suggest the  
 144 opposite; melting hinders adhesion in these experiments. Whereas melting fuses materials in welding [32]  
 145 and bonds coatings to substrates during thermal spraying [33], it can oppose adhesion in supersonic  
 146 microparticle impact. We attribute this effect to the short timescales of supersonic adhesion. If an  
 147 impacting particle resides on the top of a molten surface layer of a substrate for a long enough time, it  
 148 should eventually fuse to the substrate thanks to chemical mixing and the molten layer resolidifying. In  
 149 supersonic impact, however, the residence time of the particle on the substrate is limited. If the time  
 150 needed for solidification is longer than the residence time of the particle, it will rebound with no  
 151 mechanical resistance from the adjacent unsolidified liquid.

152

153 For an order-of-magnitude-analysis, the residence time of the particle can be estimated with the  
 154 characteristic time for a high velocity impact:

155

$$t_r = \frac{d}{V_i} \quad (1)$$

156  
 157 with  $d$  being the diameter of the particle and  $V_i$  the impact velocity. The solidification time for a thin  
 158 molten layer of volume  $v_{melt}$  limited by heat conduction of the latent heat of fusion,  $H_f$ , out through an  
 159 area  $A$  to the bulk of the substrate can be estimated using Chvorinov's rule, [34]:  
 160

$$t_s = \left[ \frac{H_f}{(T_m - T_0)} \right]^2 \left[ \frac{\rho_s \pi}{4KC} \right] \left( \frac{v_{melt}}{A} \right)^2 \quad (2)$$

161  
 162 where  $T_m$  is the melting temperature,  $T_0$  is ambient,  $K$  is the thermal conductivity of the substrate,  $\rho_s$  is the  
 163 density of the substrate, and  $C$  is the specific heat. In this analysis, for simplicity we neglect possible  
 164 superheating and changes in properties of the substrate at melting.

165 We approximate the surface area of the melt with  $A = \pi d/4^2$  and employ an energy scaling relationship to  
 166 estimate the amount of molten material produced by a hypervelocity impact following [35].

167

$$\frac{\rho_s v_{melt}}{m_p} = k \left( \frac{V_i^2}{E_m} \right)^{3\mu/2} \quad (3)$$

168  
 169 where  $m_p$  is the mass of the particle,  $k$  and  $\mu$  are scaling parameters whose values have been constrained  
 170 empirically [36,37], and  $E_m$  is the energy of the Rankine-Hugoniot state from which an adiabatic  
 171 decompression would end on the liquidus at 1 atm (see Supplemental Material [28] which includes  
 172 Refs [38,39]).

173 In Fig. 3, we compare the solidification time for the melt induced by an impact of a 14- $\mu\text{m}$  Al particle  
 174 with the residence time of the particle at different impact velocities. We present the curves for Zn and Sn  
 175 only for impact velocities beyond the corresponding threshold velocity of melting ( $\sim 1000$  and  $\sim 500$  m/s  
 176 respectively) to keep the solidification time analysis relevant. At the threshold velocity for melting, the  
 177 solidification time in both cases is at least two orders of magnitude higher than the residence time; the  
 178 molten surface layer is unable to solidify (and thereby contribute to adhesion) during the time the particle  
 179 is in contact with the substrate. At higher impact velocities the residence time only decreases, while the  
 180 solidification time rises, leading to very significant differences between the two parameters. At 1000 m/s,  
 181 for instance, the solidification times for both Zn and Sn are in the  $\mu\text{s}$  regime whereas the residence time  
 182 remains in the ns regime. Since the residence and solidification times are diverging at higher velocities in  
 183 Fig. 3, this model suggests that it is unlikely that adhesion occurs at higher impact velocities beyond those  
 184 explored in the present work.

185  
 186 Setting the residence time equal to the solidification time leads to a potential domain where there could be  
 187 a cross-over between the two:

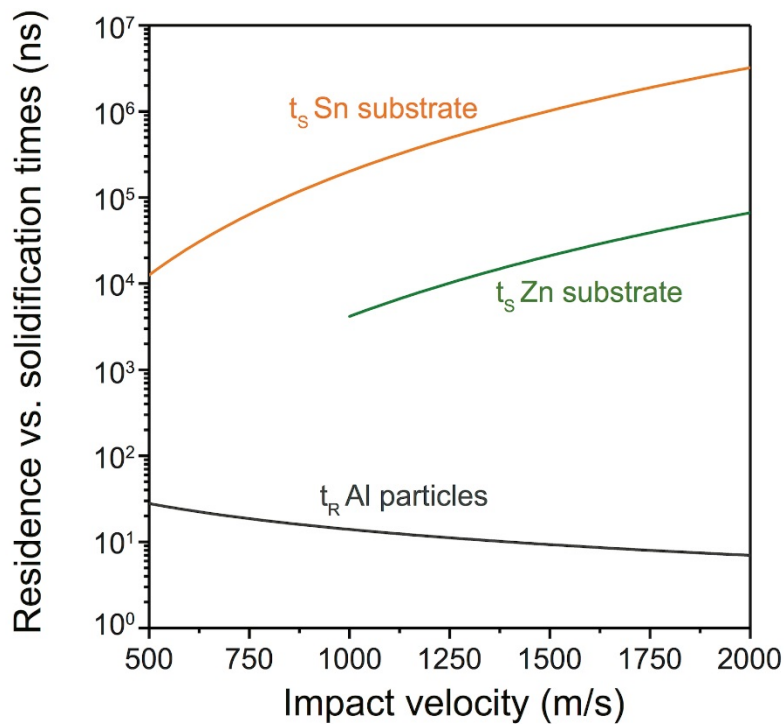
188

$$\left\{ \frac{\pi k^2 \rho_p^2}{9KC \rho_s E_m^{3\mu}} \left( \frac{H_f}{T_m - T_0} \right)^2 \right\} V_i^5 d = 1 \quad (4)$$

189

190 Equation (4) gives the locus of this crossover in the particle size-impact velocity space, with the  
191 amplitude in braces being a function of substrate properties and particle density,  $\rho_p$ . We predict based on  
192 Eq. (4) that for much smaller (submicron) particles the residence time might be long enough to  
193 accommodate solidification while the particle is in contact, which might in turn facilitate adhesion ( $t_R >$   
194  $t_S$ ) (see Fig. SM3 in Supplemental Material [28]). Although with our current platform it would be  
195 possible to launch submicron particles, such particle sizes are below the resolution of our imaging system  
196 and we would not be capable of tracking them or measuring their velocities. We offer this as a direction  
197 for future work on this topic. Although the adhesion energy does not significantly differ from one metal to  
198 another, one may also study different materials for particle and substrate to examine potential effects of  
199 the chemical nature between the two interacting materials.

200



201

202 FIG. 3. Comparison of residence time of a 14- $\mu$ m Al particle with the solidification time of the impact-  
203 induced melt in Zn and Sn substrates. The solidification time for impact-induced melting by  
204 microparticles can be orders of magnitude longer than the residence time.

205

206

207 To summarize, our *in-situ* and post-mortem observations of supersonic micro-particle impact offer a  
208 contrary viewpoint to widely postulated benefits of localized melting in impact-induces adhesion: For  $\sim 10$   
209  $\mu$ m particles, when an impact provides enough energy to melt the indent area, whether partially or fully,  
210 adhesion is found to be hindered; the low mechanical strength of the liquid interface is easily overcome  
211 by a rapidly rebounding particle if solidification is too slow to provide a solid-state joint. Such re-  
212 solidification is estimated to take orders of magnitude longer than the time that the particle resides on the



213 substrate. This mechanistic finding should prove useful for a broader understanding of impact-induced  
214 adhesion, and particularly for the design of impact-based additive manufacturing processes.

215

## 216 **Acknowledgment**

217 This work was supported by the U.S. Army through the Institute for Soldier Nanotechnologies. Funding  
218 was provided (in part) by the Army Research laboratory (Materials Manufacturing Technology Branch:  
219 RDRL-WMM-D) and by the U.S. Army Research Office, under Grant W911NF-13-D-0001. Support was  
220 also provided through Office of Naval Research DURIP Grant No. N00014-13-1-0676.

221

## 222 **References**

- 223 [1] J. E. Richardson, H. J. Melosh, and R. Greenberg, *Science* **306**, 1526 (2004).
- 224 [2] J. Blum and R. Schräpler, *Phys. Rev. Lett.* **93**, 115503 (2004).
- 225 [3] S. A. Humphry-Baker, S. Garroni, F. Delogu, and C. A. Schuh, *Nat Mater* **15**, 1280 (2016).
- 226 [4] T. Kadono and M. Arakawa, *Phys. Rev. E - Stat. Nonlinear, Soft Matter Phys.* **65**, (2002).
- 227 [5] A. Strachan, T. Cañin, and W. A. Goddard III, *Phys. Rev. B - Condens. Matter Mater. Phys.* **63**,  
228 601031 (2001).
- 229 [6] S. M. Hassani-Gangaraj, K. S. Cho, H.-J. L. Voigt, M. Guagliano, and C. A. Schuh, *Acta Mater.*  
230 **97**, 105 (2015).
- 231 [7] P. S. Branicio, R. K. Kalia, A. Nakano, and P. Vashishta, *Phys. Rev. Lett.* **96**, (2006).
- 232 [8] A. Papyrin, V. Kosarev, S. Klinkov, A. Alkhimov, and V. M. Fomin, *Cold Spray Technology*  
233 (Elsevier Science, 2006).
- 234 [9] H. Assadi, H. Kreye, F. Gärtner, and T. Klassen, *Acta Mater.* **116**, 382 (2016).
- 235 [10] A. Moridi, S. M. Hassani-Gangaraj, M. Guagliano, and M. Dao, *Surf. Eng.* **30**, 369 (2014).
- 236 [11] H. Koivuluoto, G. Bolelli, L. Lusvarghi, F. Casadei, and P. Vuoristo, *Surf. Coatings Technol.* **205**,  
237 1103 (2010).
- 238 [12] E. Sansoucy, P. Marcoux, L. Ajdelsztajn, and B. Jodoin, *Surf. Coatings Technol.* **202**, 3988  
239 (2008).
- 240 [13] A. Moridi, S. M. Hassani-Gangaraj, S. Vezzú, L. Trško, and M. Guagliano, *Surf. Coatings*  
241 *Technol.* **283**, 247 (2015).
- 242 [14] C. A. Widener, M. J. Carter, O. C. Ozdemir, R. H. Hrabe, B. Hoiland, T. E. Stamey, V. K.  
243 Champagne, and T. J. Eden, *J. Therm. Spray Technol.* **25**, 193 (2016).
- 244 [15] Y. Cormier, P. Dupuis, B. Jodoin, and A. Corbeil, *J. Therm. Spray Technol.* **25**, 170 (2016).
- 245 [16] H. Assadi, F. Gärtner, T. Stoltenhoff, and H. Kreye, *Acta Mater.* **51**, 4379 (2003).
- 246 [17] T. Schmidt, F. Gärtner, H. Assadi, and H. Kreye, *Acta Mater.* **54**, 729 (2006).
- 247 [18] W.-Y. Li, C.-J. Li, and H. Liao, *Appl. Surf. Sci.* **256**, 4953 (2010).

- 248 [19] S. Guetta, M. H. Berger, F. Borit, V. Guipont, M. Jeandin, M. Boustie, Y. Ichikawa, K. Sakaguchi,  
249 and K. Ogawa, *J. Therm. Spray Technol.* **18**, 331 (2009).
- 250 [20] G. Bae, S. Kumar, S. Yoon, K. Kang, H. Na, H.-J. Kim, and C. Lee, *Acta Mater.* **57**, 5654 (2009).
- 251 [21] M. Grujicic, C. L. Zhao, W. S. DeRosset, and D. Helfrich, *Mater. Des.* **25**, 681 (2004).
- 252 [22] W.-Y. Li, C. Zhang, H.-T. Wang, X. P. Guo, H. L. Liao, C.-J. Li, and C. Coddet, *Appl. Surf. Sci.*  
253 **253**, 3557 (2007).
- 254 [23] V. K. Champagne, M. K. West, M. Reza Rokni, T. Curtis, V. Champagne, and B. McNally, *J.*  
255 *Therm. Spray Technol.* **25**, 143 (2016).
- 256 [24] M. V. Vidaller, A. List, F. Gaertner, T. Klassen, S. Dosta, and J. M. Guilemany, *J. Therm. Spray*  
257 *Technol.* **24**, 644 (2015).
- 258 [25] P. C. King, C. Busch, T. Kittel-Sherri, M. Jahedi, and S. Gulizia, *Surf. Coatings Technol.* **239**, 191  
259 (2014).
- 260 [26] M. Hassani-Gangaraj, D. Veysset, K. A. Nelson, and C. A. Schuh, arXiv:1612.08081 (2016).
- 261 [27] D. Veysset, A. J. Hsieh, S. Kooi, A. A. Maznev, K. A. Masser, and K. A. Nelson, *Sci. Rep.* **6**,  
262 25577 (2016).
- 263 [28] See Supplemental Material [url] for sample preparation, coefficient of restitutions for Al  
264 microparticle impacts on Sn, EDS analysis, calculations of the energy term for melt volume  
265 analysis as well as solidification and residence time ratio maps for Al particle impacting Zn and  
266 Sn. Supplemental Material includes Refs. [38,39].
- 267 [29] D. H. Sharp, *Phys. D Nonlinear Phenom.* **12**, 3 (1984).
- 268 [30] H. Okamoto, *Desk Handbook: Phase Diagrams for Binary Alloys* (ASM International, 2010).
- 269 [31] L. Vitos, A. V Ruban, H. L. Skriver, and J. Kollár, *Surf. Sci.* **411**, 186 (1998).
- 270 [32] V. Avagyan, *Phys. Rev. Spec. Top. - Accel. Beams* **9**, (2006).
- 271 [33] H. Herman, S. Sampath, and R. McCune, *MRS Bull.* **25**, 17 (2000).
- 272 [34] J. Campbell, *Complete Casting Handbook: Metal Casting Processes, Metallurgy, Techniques and*  
273 *Design* (Elsevier Science, 2015).
- 274 [35] M. D. Bjorkman and K. A. Holsapple, *Int J Impact Eng* **5**, (1987).
- 275 [36] E. Pierazzo, A. M. Vickery, and H. J. Melosh, *Icarus* **127**, (1997).
- 276 [37] J. de Vries, F. Nimmo, H. J. Melosh, S. A. Jacobson, A. Morbidelli, and D. C. Rubie, *Prog. Earth*  
277 *Planet. Sci.* **3**, 7 (2016).
- 278 [38] M. A. Meyers, *Dynamic Behavior of Materials* (John Wiley & Sons, New York, 1994).
- 279 [39] M. B. Rubin and A. L. Yarin, *Int. J. Impact Eng.* **27**, 387 (2002).
- 280